MÖSSBAUER SPECTROSCOPY STUDY OF $MgAl_2O_4$-MATRIX NANOCOMPOSITE POWDERS CONTAINING CARBON NANOTUBES AND IRON-BASED NANOPARTICLES

P. COQUAY[1]†, E. DE GRAVE[1], R. E. VANDENBERGHE[1], C. DAUWE[1], E. FLAHAUT[2], CH. LAURENT[2], A. PEIGNEY[2] and A. ROUSSET[2]

[1]NUMAT, Department of Subatomic and Radiation Physics, University of Gent, Proeftuinstraat 86, B-9000 Gent, Belgium and [2]CIRIMAT, UMR CNRS 5085, Laboratoire de Chimie des Matériaux Inorganiques, Université Paul-Sabatier, 31062 Toulouse cedex 4, France

Abstract—Materials involved in the catalytic formation of carbon nanotubes are for the first time systematically studied by Mössbauer spectroscopy between 11 K and room temperature. $Mg_{1-x}Fe_xAl_2O_4$ ($x = 0.1$, 0.2, 0.3, 0.4) solid solutions are transformed into carbon nanotubes–Fe/Fe_3C–$MgAl_2O_4$ composite powders by reduction in a H_2–CH_4 gas mixture. The oxides are defective spinels of general formulae $(Mg^{2+}_{1-x}Fe^{2+}_{x-3\alpha}Fe^{3+}_{2\alpha}\square_\alpha Al^{3+}_2)O^{2-}_4$. Ferromagnetic α-Fe, ferromagnetic Fe_3C and a γ-Fe form, the latter possibly corresponding to a γ-Fe–C alloy, are detected in the composite powders. An attempt is made to correlate these results with the microstructure of the powder. It seems that the nanoparticles, which catalyze the formation of the carbon nanotubes, are detected as Fe_3C in the post-reaction Mössbauer spectroscopy analysis.

Résumé—Des matériaux impliqués dans la formation catalytique de nanotubes de carbone sont pour la première fois systématiquement étudiés par spectroscopie Mössbauer entre 11 K et la température ambiante. Des solutions solides $Mg_{1-x}Fe_xAl_2O_4$ ($x = 0.1$, 0.2, 0.3, 0.4) sont transformées en poudres composites nanotubes de carbone–Fe/Fe_3C–$MgAl_2O_4$ par réduction dans un mélange gazeux de H_2 et de CH_4. Les oxydes sont des spinelles lacunaires de formule générale $(Mg^{2+}_{1-x}Fe^{2+}_{x-3\alpha}Fe^{3+}_{2\alpha}\square_\alpha Al^{3+}_2)O^{2-}_4$. Du Fe-α ferromagnétique, du Fe_3C ferromagnétique et une forme de Fe-γ, cette dernière correspondant probablement à un alliage Fe–C-γ, sont détectés dans les poudres composites. Des corrélations sont faites entre ces résultats et la microstructure de la poudre. Il semble que les nanoparticules qui catalysent la formation des nanotubes de carbone sont détectées comme du Fe_3C dans l'analyse par spectroscopie Mössbauer des produits obtenus après la réaction.

Keywords: Carbon nanotubes; Iron; Carbides; Mössbauer effect

1. INTRODUCTION

Since the report by Iijima [1] on carbon nanotubes (hereafter denoted as C_{NTs}), many laboratories around the world have been studying this new form of carbon which presents high expectations for future applications such as light-weight composite materials, hydrogen storage and lithium-ion batteries. Methods of synthesis have been reviewed by Journet and Bernier [2]. Several of these involve nanometric metal particles as catalysts. Laurent *et al.* [3] have surveyed the various mechanisms proposed for nanotube nucleation and growth from such particles. In particular, the catalytic decomposition of hydrocarbons or the disproportionation of CO on metal particles (generally based on Fe, Co or Ni) lead to Iijima-type C_{NTs}, as opposed to hollow carbon fibers, when the catalyst particles are sufficiently small [4–9]. Some works [8, 10, 11] have shown that the active particles are smaller than *c.* 6 nm in diameter. Catalytic methods are promising owing to the possibilities of up-scaling but one difficulty is to obtain the nanometric particles at the relatively high temperature (usually higher than 800°C) required for the formation of C_{NTs}.

Works by some of the present authors [5, 10–15]

† To whom all correspondence should be addressed. Tel.: +1-32-92646569; fax: +1-32-92646697; *E-mail:* pierre.coquay@ny.ac.be (P. Coquay).

have shown that single-wall nanotubes (SWNTs) and small multi-wall nanotubes (MWNTs) are advantageously prepared by the selective reduction of oxide solid solutions in H_2–CH_4 gas mixtures. The reduction of a solid solution between a non-reducible oxide such as Al_2O_3, $MgAl_2O_4$ or MgO and one or more transition metal oxide(s) produces very small transition metal (Fe, Co, Ni and their alloys) nanoparticles at a temperature usually higher than 800°C. The decomposition of CH_4 over the freshly formed metal nanoparticles prevents their further growth and thus results in the very strong proportion of SWNTs and small MWNTs compared with other forms of carbon.

C_{NTs}–Fe/Fe_3C–$MgAl_2O_4$ powders were prepared by reduction in H_2–CH_4 atmosphere of $Mg_{1-x}Fe_xAl_2O_4$ ($x = 0.1$, 0.2, 0.3, 0.4) solid solutions. Results on the synthesis and microstructure of these powders have been published earlier [15] but detailed information on the Fe species that could be responsible for the formation of the C_{NTs} is lacking. The present paper reports a study by ^{57}Fe Mössbauer spectroscopy of the oxide solid solutions and of the corresponding reduced powders.

2. EXPERIMENTAL

The $Mg_{1-x}Fe_xAl_2O_4$ ($x = 0.1$, 0.2, 0.3, 0.4) solid solutions were prepared by the combustion route as described elsewhere [15]. Briefly, the appropriate amounts of the desired metal nitrates (Mg, Al, and Fe) were mixed in stoichiometric proportions with urea and dissolved in a minimum amount of water. The solutions were then placed in a furnace pre-heated at 600°C, where the autocatalytic exothermic redox reaction takes place within minutes, producing the oxide powder. These powders were then attrition-milled. In the next step, the oxide solid solutions obtained were reduced in a H_2–CH_4 gas mixture (18 mol% CH_4) for 6 min at 1070°C, giving rise to the C_{NTs}–Fe/Fe_3C–$MgAl_2O_4$ composite powders. For the sake of brevity, the samples will be referred to according to the following example: the solid solution $Mg_{0.9}Fe_{0.1}Al_2O_4$ will be named Mg9Fe1 and the corresponding composite powder Mg9Fe1R, where R stands for "reduced".

The ^{57}Fe Mössbauer spectra were recorded with ^{57}Co (Rh) sources in a conventional time-mode spectrometer with constant-acceleration drive and a triangular reference signal. Accumulation of the data was performed in 1024 channels until a background of at least 10^6 counts per channel was reached. The spectrometer was calibrated by collecting at room temperature (RT) the spectrum of a standard α-Fe foil and the isomer-shift values quoted hereafter are with reference to this standard. The spectra of the nanocomposite powders were analyzed assuming symmetrical components with a Lorentzian line shape, while those of the oxide powders were fitted with a quadrupole-shift distribution where each subspectrum is composed of Lorentzian lines. Most of the spectra were recorded at 80 K and at RT to detect a possible evolution of the Fe phases. In addition, selected specimens were examined at different temperatures between 11 K and RT.

3. RESULTS AND DISCUSSION

3.1. Oxide solid solutions

Previous analyses [15] have revealed that only a spinel phase is detected in the X-ray diffraction (XRD) patterns. The Mössbauer spectra of the oxide solid solutions were recorded at 80 K. The corresponding parameters are reported in Table 1 and a typical spectrum is shown in Fig. 1(a).

The spectra were fitted with two distributed doublets, characteristic of ferrous and ferric iron. A slightly better fit is obtained in the case of Mg9Fe1 by adding a linear correlation between the isomer shift and the quadrupole splitting in the distribution for both doublets, as it was previously shown for similar oxides [16]. This correlation does not give a better result for the powders containing more iron and thus was not used in the corresponding fits. For these powders, the isomer-shift values given in Table 1 are average values. In both distributions of quadrupole splittings two main components may be recognized [Figs 1(b) and (c)]. Since the spinel lattice has octahedral and tetrahedral sites, the two peaks in the distribution profiles for both the Fe^{2+} and Fe^{3+} components could indicate that both cations are distributed among these two lattice sites. However, this is difficult to ascertain due to the inaccuracy of the calculated quadrupole-splitting distributions, and hence possible artefacts. The presence of Fe^{3+} in the lattice of $MgAl_2O_4$ indicates that the obtained products are defective spinels, whose formulae can be written as $(Mg^{2+}_{1-x}Fe^{2+}_{x-3\alpha}Fe^{3+}_{2\alpha}\square_\alpha Al^{3+}_2)O^{2-}_4$ ($0.1 \le x \le 0.4$).

Table 1. 80 K Mössbauer parameters of the Mg9Fe1, Mg8Fe2, Mg7Fe3 and Mg6Fe4 oxide powders. Para: paramagnetic; δ: isomer shift (mm/s); ΔE_Q: quadrupole splitting (mm/s); Γ: line width (mm/s) of elemental doublet; P: proportion (%); (1) and (2) refer to the two components which are recognized in the respective probability distribution profiles

		Para Fe^{2+}				Para Fe^{3+}			
		δ	ΔE_Q	Γ	P	δ	ΔE_Q	Γ	P
Mg9Fe1	(1)	1.09	2.0	0.30	38	0.38	0.8	0.63	62
	(2)	1.05	2.9			0.49	1.8		
Mg8Fe2	(1)	1.05	2.0	0.32	43	0.38	0.9	0.36	57
	(2)		2.9				2.0		
Mg7Fe3	(1)	1.03	2.0	0.40	47	0.40	0.9	0.40	53
	(2)		2.75				1.8		
Mg6Fe4	(1)	1.04	1.95	0.37	48	0.39	0.9	0.26	52
	(2)		3.0				1.9		

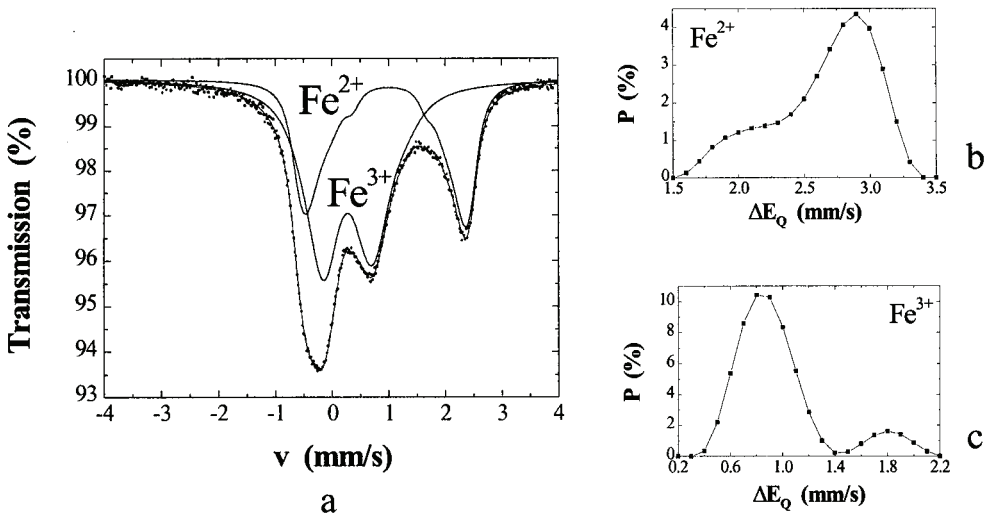

Fig. 1. 80 K Mössbauer spectrum of the Mg9Fe1 oxide powder (a) and quadrupole-splitting distributions of the Fe^{2+} (b) and Fe^{3+} (c) doublets.

3.2. Nanocomposite powders

XRD-pattern analysis of the composite powders [15] has revealed the presence of α-Fe and Fe_3C in addition to the spinel matrix. However, no γ-Fe could be resolved, possibly due to the superposition of its peaks with those of the major phases. Scanning electron microscopy (SEM) observations [15] have shown that the metal-oxide grains are uniformly covered by a web-like network of C_{NTs} bundles, several tens of micrometers long. A typical SEM image referring to powder Mg8Fe2R is represented in Fig. 2(a). It has been observed in transmission electron microscopy (TEM) [Fig. 2(b)] that the bundles are made up of SWNTs and small MWNTs with a diameter close to 4 nm. Carbon-coated particles of an unidentified nature (metallic iron, iron–carbon alloy or iron carbide) in the 5–20 nm size range were found at the surface of the C_{NTs}, as opposed to inside the C_{NTs}, and were therefore not thought to be related to the processes of C_{NTs} formation. In contrast, smaller particles were occasionally found inside the tube tips. It is also important to note that the reduction of the ferrous and ferric ions produces particles inside the spinel grains.

The characteristic parameters of the Mössbauer spectra recorded at RT and at 80 K are reported in Tables 2 and 3, respectively. Typical spectra are shown in Fig. 3. The fits consist of four patterns: one doublet, two sextets and one singlet. The doublet at RT is characteristic of an Fe^{2+} phase. However, it could not be reasonably adjusted in the spectra at 80 K. The larger sextet is due to ferromagnetic α-Fe particles and the narrower one is characteristic of ferromagnetic Fe_3C (cementite). Since Fe_3C has two inequivalent crystallographic sites [17], the Mössbauer parameters of the sextet accounting for Fe_3C correspond to the average of the two Fe-site parameters. The values obtained at RT and at 80 K are in good agreement with those

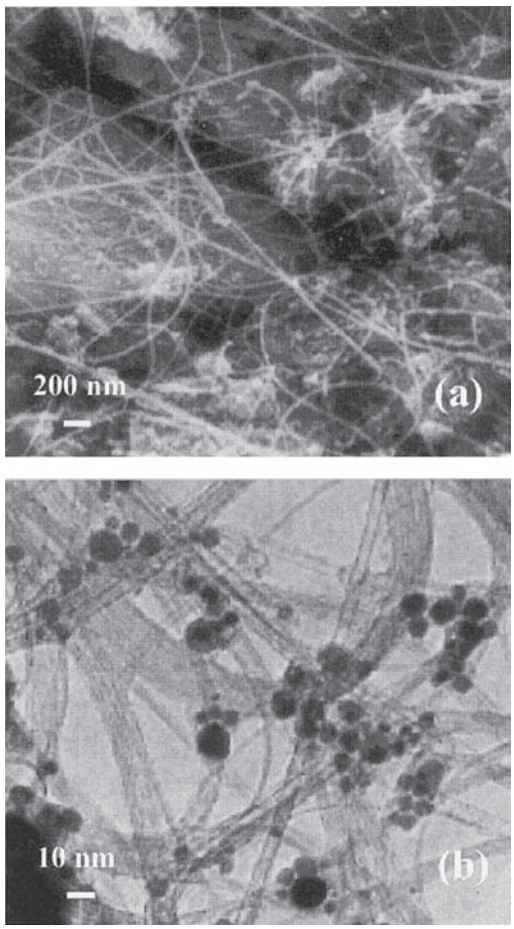

Fig. 2. SEM (a) and TEM (b) images of the Mg8Fe2R nanocomposite powder.

Table 2. RT Mössbauer parameters of the Mg9Fe1R, Mg8Fe2R, Mg7Fe3R and Mg6Fe4R nanocomposite powders. Para: paramagnetic; ferro: ferromagnetic; H_{hf}: hyperfine field (kOe); δ: isomer shift (mm/s); ΔE_Q: quadrupole splitting (mm/s); $2\varepsilon_Q$: quadrupole shift (mm/s); Γ: line width (mm/s); P: proportion (%)

	Para Fe^{2+}				Ferro α-Fe					Ferro Fe_3C					Non-ferro Fe		
	δ	ΔE_Q	Γ	P	δ	H_{hf}	$2\varepsilon_Q$	Γ	P	δ	H_{hf}	$2\varepsilon_Q$	Γ	P	δ	Γ	P
Mg9Fe1R	1.19	0.85	0.69	2.5	0	331	0[a]	0.28	47	0.18	205	0.026	0.34	27.5	−0.089	0.32	23
Mg8Fe2R	1.09	1.19	0.48	2	0	332	0[a]	0.27	28	0.18	206	0.022	0.28	56	−0.085	0.33	14
Mg7Fe3R	1.15	1.36	0.49	2	0	331	0[a]	0.28	24	0.18	206	0.019	0.29	58	−0.092	0.32	16
Mg6Fe4R	1.16	1.46	0.34	1.5	0	331	0[a]	0.26	21.5	0.18	206	0.027	0.27	52	−0.095	0.28	25

[a] Fixed parameter.

Table 3. 80 K Mössbauer parameters of the Mg9Fe1R, Mg8Fe2R, Mg7Fe3R and Mg6Fe4R nanocomposite powders. Ferro: ferromagnetic; H_{hf}: hyperfine field (kOe); δ: isomer shift (mm/s); $2\varepsilon_Q$: quadrupole shift (mm/s); Γ: line width (mm/s); P: proportion (%)

	Ferro α-Fe					Ferro Fe_3C					Non-ferro Fe		
	δ	H_{hf}	$2\varepsilon_Q$	Γ	P	δ	H_{hf}	$2\varepsilon_Q$	Γ	P	δ	Γ	P
Mg9Fe1R	0.12	342	0[a]	0.31	44	0.30	247	~0	0.34	31.5	0.037	0.58	24.5
Mg8Fe2R	0.12	343	0[a]	0.29	27.5	0.31	248	~0	0.32	59	0.031	0.51	13.5
Mg7Fe3R	0.11	342	0[a]	0.28	21.5	0.31	247	~0	0.31	62.5	0.016	0.40	16
Mg6Fe4R	0.11	340	0[a]	0.29	21	0.31	247	~0	0.31	54	0.017	0.36	25

[a] Fixed parameter.

reported by Bi *et al.* [18] for Fe_3C nanoparticles. Regarding the singlet, the negative value of the isomer shift at RT suggests a γ-Fe phase.

The Mössbauer spectra of Mg9Fe1R and Mg6Fe4R were recorded at various temperatures between 11 K and RT (Tables 4 and 5, respectively—Fig. 4). Again, the weak Fe^{2+} doublet could not be resolved at low temperatures. However, even using a larger velocity scale, no new sextet could be detected at these temperatures. This paramagnetic oxide phase could reflect the presence of Fe^{2+} ions distributed in the spinel lattice, indicating that the starting oxide solid solutions are not fully reduced under the chosen conditions. The obtained Mössbauer parameters are in agreement with this conclusion and the expected values of the isomer shift and quadrupole splitting at low temperatures suggest that this weak doublet is completely obscured by the more intense pattern of the Fe_3C sextet. Considering this, no significant evolution of the proportions of the different Fe phases can be detected. Nevertheless, referring to the proportions of the Fe phases at RT (Table 2) where the Fe^{2+} doublet is clearly resolved, relative errors of $\pm 2.5\%$, $\pm 4\%$ and $\pm 1.5\%$ are estimated for the proportions of α-Fe, Fe_3C and the singlet, respectively. These considerations based on the variations of the proportion values reported in Table 4 reasonably include the uncertainties of the fits.

A considerable broadening of the singlet at low temperatures is clearly observed. For these temperatures, a narrow sextet was used instead of a singlet to fit the spectra, yielding a more adequate reproduction of the central part of the spectra. This could indicate that the corresponding Fe-species undergo a paramagnetic–antiferromagnetic transformation with a transition temperature at about 75 and 50 K for Mg9Fe1R and Mg6Fe4R, respectively. This also suggests a γ-Fe phase since it is known that paramagnetic γ-Fe shows an antiferromagnetic coupling below 80 K [19]. The hyperfine fields (Tables 4 and 5) are in good agreement with the saturation field (27 ± 5 kOe) reported by Crowell and Walker for small antiferromagnetic γ-Fe–Ni particles [20].

The present results are to be compared with those resulting from a study of Fe–$MgAl_2O_4$ powders prepared by reduction in an atmosphere of pure H_2 [16]. Obviously no carbides, nor C_{NTs}, were formed in those powders. Mössbauer spectroscopy analysis has revealed two phases: the sextet characteristic of ferromagnetic α-Fe is detected at all temperatures between 9 and 298 K and a singlet appears above 50 K. The singlet was assigned to paramagnetic α-Fe in the form of very small nanoparticles with a lowered Curie temperature. It was furthermore shown that the latter particles were intragranularly dispersed in the spinel matrix.

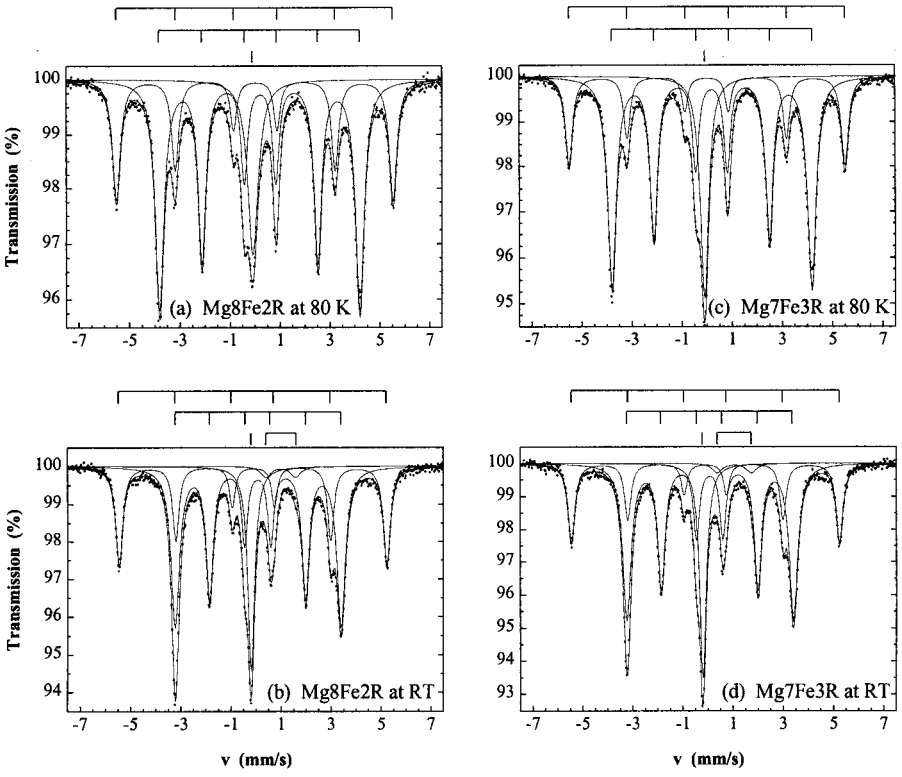

Fig. 3. 80 K (a) and RT (b) Mössbauer spectra of the Mg8Fe2R nanocomposite powder and 80 K (c) and RT (d) spectra of the Mg7Fe3R nanocomposite powder.

Table 4. Mössbauer parameters of Mg9Fe1R between 11 K and RT. Para: paramagnetic; ferro: ferromagnetic; antiferro: antiferromagnetic; H_{hf}: hyperfine field (kOe); δ: isomer shift (mm/s); ΔE_Q: quadrupole splitting (mm/s); $2\varepsilon_Q$: quadrupole shift (mm/s); Γ: line width (mm/s); P: proportion (%)

	Para Fe^{2+}				Ferro α-Fe					Ferro Fe_3C					Antiferro/para γ-Fe–C				
T	δ	ΔE_Q	Γ	P	δ	H_{hf}	$2\varepsilon_Q$	Γ	P	δ	H_{hf}	$2\varepsilon_Q$	Γ	P	δ	H_{hf}	$2\varepsilon_Q$	Γ	P
11	–	–	–	–	0.13	343	0[a]	0.34	45	0.31	252	∼0	0.35	31.5	0.043	18.5	0[a]	0.56	23.5
30	–	–	–	–	0.12	343	0[a]	0.34	44.5	0.31	252	∼0	0.35	31.5	0.038	17	0[a]	0.57	24
50	–	–	–	–	0.13	343	0[a]	0.35	44.5	0.31	251	∼0	0.37	31	0.038	15	0[a]	0.57	24.5
75	–	–	–	–	0.12	342	0[a]	0.36	45	0.30	248	∼0	0.36	30.5	0.040	10	0[a]	0.54	24.5
100	1.01	2.03	0.52	1.5	0.11	342	0[a]	0.34	45	0.30	246	∼0	0.36	30	0.030	–	–	0.49	23.5
125	1.22	1.41	0.77	2	0.10	340	0[a]	0.32	45	0.29	242	∼0	0.38	30	0.016	–	–	0.41	23
150	1.31	1.65	0.56	2	0.092	339	0[a]	0.34	45	0.28	238	∼0	0.36	30	0.003	–	–	0.40	23
175	1.18	1.24	0.66	2.5	0.078	338	0[a]	0.33	44.5	0.26	235	∼0	0.42	28.5	0	–	–	0.40	24.5
200	1.21	1.39	0.47	2	0.067	337	0[a]	0.35	45	0.26	230	∼0	0.41	28.5	−0.018	–	–	0.41	24.5
225	1.24	1.48	0.56	3	0.046	335	0[a]	0.34	46	0.24	226	∼0	0.41	27	−0.032	–	–	0.39	24
250	1.10	1.21	0.48	3	0.032	334	0[a]	0.39	45	0.23	219	0.019	0.43	28	−0.045	–	–	0.39	24
275	1.07	1.03	0.52	3	0.017	332	0[a]	0.36	47	0.21	213	0.018	0.41	26	−0.066	–	–	0.39	24
295	1.13	1.13	0.51	3	0	331	0[a]	0.36	48	0.20	206	0.016	0.38	25	−0.079	–	–	0.40	24

[a] Fixed parameter.

Table 5. Mössbauer parameters of Mg6Fe4R between 16 and 200 K. Ferro: ferromagnetic; antiferro: antiferromagnetic; para: paramagnetic; H_{hf}: hyperfine field (kOe); δ: isomer shift (mm/s); $2\varepsilon_Q$: quadrupole shift (mm/s); Γ: line width (mm/s); P: proportion (%)

	Ferro α-Fe					Ferro Fe_3C					Antiferro/para γ-Fe–C				
T	δ	H_{hf}	$2\varepsilon_Q$	Γ	P	δ	H_{hf}	$2\varepsilon_Q$	Γ	P	δ	H_{hf}	$2\varepsilon_Q$	Γ	P
16	0.12	341	0[a]	0.42	21.5	0.31	251	∼0	0.35	53	0.026	9	0[a]	0.46	25.5
30	0.12	341	0[a]	0.41	22	0.31	250	∼0	0.36	52.5	0.023	7	0[a]	0.44	25.5
50	0.12	341	0[a]	0.38	22	0.31	249	0.01	0.37	53	0.019	6	0[a]	0.40	25
75	0.11	340	0[a]	0.44	22	0.31	247	∼0	0.36	53	0.020	–	–	0.44	25
100	0.11	340	0[a]	0.47	23	0.30	245	∼0	0.38	52	0.011	–	–	0.43	25
125	0.10	339	0[a]	0.39	22.5	0.29	242	∼0	0.36	53	0	–	–	0.39	24.5
200	0.06	336	0[a]	0.44	23	0.25	231	0.01	0.38	52	−0.035	–	–	0.41	25

[a] Fixed parameter.

It is proposed that the singlet in the current spectra, being present at temperatures as low as 11 K with an unchanged proportion, could reflect the formation of a γ-Fe–C phase. Indeed, in addition to the nanosize of the particles [21], a small proportion of carbon added to iron (austenite) could also hinder the martensitic transformation of γ-Fe to α-Fe [22], which takes place at 910°C for pure bulk iron. The lower Néel temperature and the lower values of the hyperfine field observed for Mg6Fe4R compared with Mg9Fe1R (Tables 4 and 5) could be a consequence of slight differences in carbon content. A comparison with the Mössbauer parameters reported by Bauer *et al.* [23] for γ-Fe–C bulk materials indicates that the hyperfine interaction is characteristic of an iron atom with carbon atoms farther away than the next-nearest neighbor positions.

The absence in the present spectra of the paramagnetic α-Fe phase detected by Quénard [16] could indicate that at least a part of the corresponding intragranular particles are found in the form of γ-Fe–C species in the present materials. A study on C_{NTs}–Fe/Fe_3C–Al_2O_3 composite powders [10] has indeed shown that γ-Fe (possibly γ-Fe–C) species were located in the intragranular position. This suggests that a fraction of the carbon supplied by the decomposition of CH_4 migrates inside the lattice of the oxide matrix.

It has been shown [15] that the total carbon content in the C_{NTs}–Fe/Fe_3C–$MgAl_2O_4$ composite powders increases steadily with the proportion of

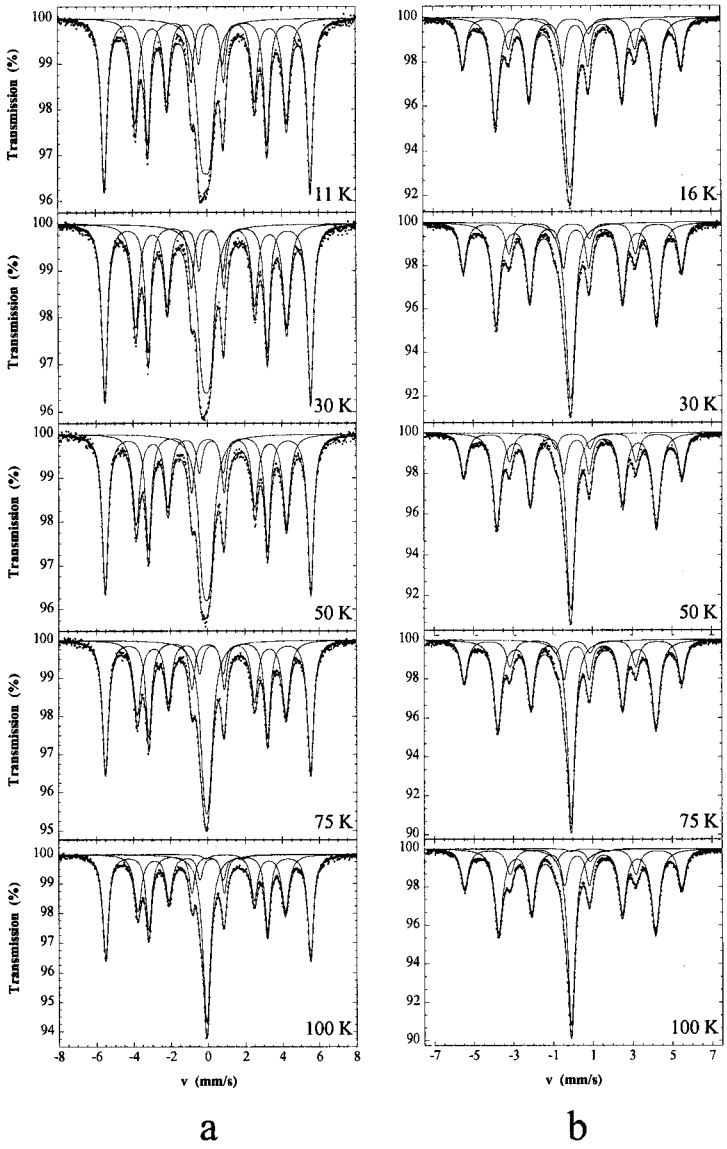

Fig. 4. Mössbauer spectra of the Mg9Fe1R (a) and Mg6Fe4R (b) nanocomposite powders measured at different temperatures.

iron and that the quantity of C_{NTs} strongly increases between Mg9Fe1R and Mg8Fe2R, reaching saturation for Mg7Fe3R (Fig. 5). The evolution between Mg9Fe1R and Mg8Fe2R could reflect the higher density of potentially active particles at the surface of the matrix grains upon the increase of the total iron content. For specimens with a higher iron content (Mg7Fe3R and Mg6Fe4R), this is balanced by an easier coalescence, and hence deactivation, of the surface particles.

The proportions of the different Fe phases present in the composite powders as revealed by the RT Mössbauer spectra (Table 2) are shown in Fig. 6(a). The proportion of Fe_3C roughly doubles from *c.* 30% to *c.* 60% between Mg9Fe1R and Mg8Fe2R and subsequently reaches saturation. The fraction of α-Fe follows an almost opposite evolution whereas the γ-Fe–C proportion initially decreases and then increases again so that it is similar for Mg9Fe1R and Mg6Fe4R. Figure 6(b) shows the amounts of the different Fe phases present in the samples. To obtain a reasonable approximation of the amounts from the proportions, the latter were multiplied by one, two, three and four for Mg9Fe1R, Mg8Fe2R, Mg7Fe3R and Mg6Fe4R, respectively. The relative errors were multiplied in the same way. The contents of both Fe_3C and α-Fe steadily increase with the iron content, the former one in a much more pronounced way. In contrast, the γ-Fe–C content is the same for Mg9Fe1R and Mg8Fe2R and only increases for higher amounts of iron.

These results seem to indicate that the particles responsible for the nucleation and possibly the growth of the C_{NTs} are found as Fe_3C by post-reaction Mössbauer spectroscopy analyses. The exact nature of the catalytic particle is not known but it is probably a very small carbon-containing Fe particle in which some still poorly established driving forces make carbon atoms participate in the formation of the C_{NTs}. However, the continuous increase of the Fe_3C quantity [Fig. 6(b)] indicates that some of the particles located at the surface of the spinel grains that were inactive for the formation of the C_{NTs} also end up as cementite. The continuous increase of the quantities of α-Fe and γ-Fe–C could further indicate that such inactive particles are detected as α-Fe and γ-Fe–C in post-reaction Mössbauer spectra. The difference in the post-reaction nature of the particles probably reflects the size distribution (5–20 nm) observed by TEM [15]. The relative thickness of the carbon coating compared with the size of a given particle could influence its post-reaction nature.

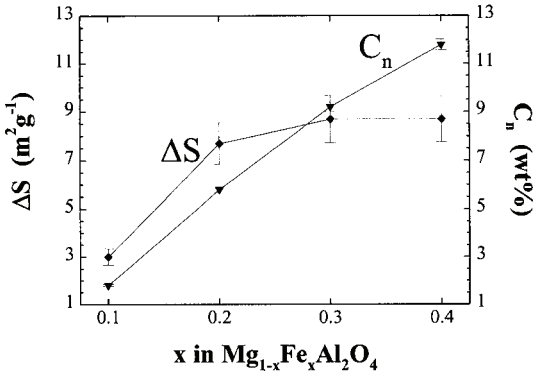

Fig. 5. Carbon content (C_n) and quantity factor of carbon nanotubes (ΔS) in the composite powders. ΔS represents the surface area of carbon in the composite powder, which essentially corresponds to that of the C_{NTs}. See Ref. [15] for details. The lines are guides to the eye.

4. CONCLUSIONS

$Mg_{1-x}Fe_xAl_2O_4$ ($x = 0.1$, 0.2, 0.3, 0.4) solid solutions were transformed into C_{NTs}–Fe/Fe_3C–$MgAl_2O_4$ composite powders by reduction in a H_2–CH_4 gas mixture. Materials involved in the catalytic formation of carbon nanotubes were for the first time systematically studied by Mössbauer spectroscopy between 11 K and room temperature. The study has shown that the primary oxides are defective spinels of general formulae

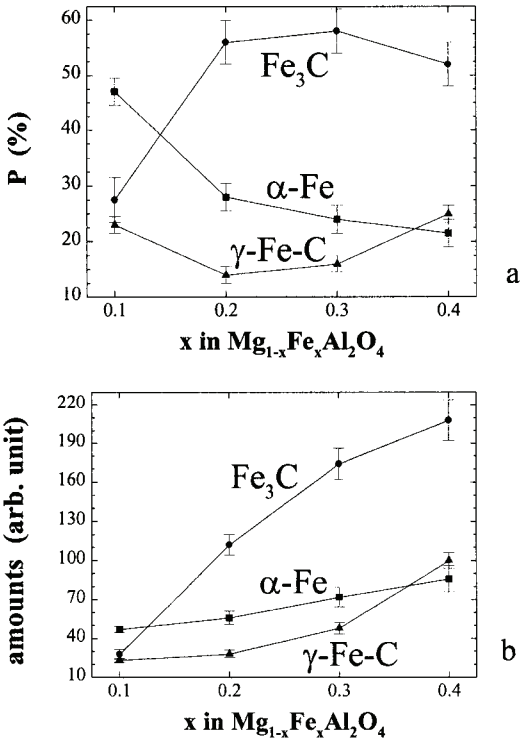

Fig. 6. Proportions of the different Fe phases present in the composite powders as revealed by the Mössbauer spectra at RT (a) and corresponding amounts of the different Fe phases in the powders (b). The amounts were obtained by multiplying the corresponding proportions by one, two, three and four for Mg9Fe1R, Mg8Fe2R, Mg7Fe3R and Mg6Fe4R, respectively. The lines are guides to the eye.

$(Mg^{2+}_{1-x}Fe^{2+}_{x-3\alpha}Fe^{3+}_{2\alpha}\square_{\alpha}Al^{3+}_{2})O^{2-}_{4}$ $(0.1 \leq x \leq 0.4)$. Different Fe phases have been detected in the composite powders: ferromagnetic α-Fe, ferromagnetic Fe_3C and a γ-Fe form that could correspond to a γ-Fe–C alloy. It has been attempted to correlate these results with the microstructure of the powder. This study suggests (i) that the particles that catalyze the formation of the C_{NTs} are Fe_3C in post-reaction examinations, (ii) that the particles located inside the spinel grains are mostly in the γ-Fe–C form, and (iii) that the inactive carbon-coated particles could end up as any of the α-Fe, Fe_3C and γ-Fe–C forms.

Acknowledgements—This work was partly funded by the Belgian National Programme of Inter-University Attraction Pole on Reduced Dimensionality Systems (PAI–IUAP P4/10) and by the Fund for Scientific Research, Flanders. The franco-belgian TOURNESOL program (project T99.006) is also gratefully acknowledged.

REFERENCES

1. Iijima, S., *Nature*, 1991, **354**, 56.
2. Journet, C. and Bernier, P., *Appl. Phys. A*, 1998, **67**, 1.
3. Laurent, Ch., Flahaut, E., Peigney, A. and Rousset, A., *New J. Chem*., 1998, **22**, 1229.
4. Dai, H., Rinzler, A. G., Nikolaev, P., Thess, A., Colbert, D. T. and Smalley, R. E., *Chem. Phys. Lett*., 1996, **260**, 471.
5. Peigney, A., Laurent, Ch., Dobigeon, F. and Rousset, A., *J. Mater. Res*., 1997, **12**, 613.
6. Kong, J., Cassell, A. M. and Dai, H., *Chem. Phys. Lett*., 1998, **292**, 567.
7. Cheng, H. M., Li, F., Sun, X., Brown, S. D. M., Pimenta, A., Marucci, A., Dresselhaus, G. and Dresselhaus, M. S., *Chem. Phys. Lett*., 1998, **289**, 602.
8. Hafner, J. H., Bronikowski, M. J., Azamian, B. K., Nikolaev, P., Rinzler, A. G., Colbert, D. T., Smith, K. A. and Smalley, R. E., *Chem. Phys. Lett*., 1998, **296**, 195.
9. Colomer, J. F., Bister, G., Willems, I., Konya, Z., Fonseca, A., Van Tendeloo, G. and Nagy, J. B., *Chem. Commun*., 1999, 1343.
10. Peigney, A., Laurent, Ch. and Rousset, A., *J. Mater. Chem*., 1999, **9**, 1167.
11. Flahaut, E., Peigney, A., Laurent, Ch., Rousset, A., *J. Mater. Chem*., 2000, **10**, 249.
12. Laurent, Ch., Peigney, A. and Rousset, A., *J. Mater. Chem*., 1998, **8**, 1263.
13. Peigney, A., Laurent, Ch., Dumortier, O. and Rousset, A., *J. Eur. Ceram. Soc*., 1998, **18**, 1995.
14. Flahaut, E., Govindaraj, A., Peigney, A., Laurent, Ch., Rousset, A. and Rao, C. N. R., *Chem. Phys. Lett*., 1999, **300**, 236.
15. Govindaraj, A., Flahaut, E., Laurent, Ch., Peigney, A., Rousset, A. and Rao, C. N. R., *J. Mater. Res*., 1999, **14**, 2567.
16. Quénard, O., Doctoral thesis, Toulouse, 1997, p. 283.
17. Yakel, H. L., *Int. metall. Rev*., 1985, **30**, 17.
18. Bi, X. X., Ganguly, B., Huffman, G. P., Huggins, F. E., Endo, M. and Eklund, P. C., *J. Mater. Res*., 1993, **8**, 1666.
19. Weiss, R. J., *Proc. Phys. Soc*., 1963, **82**, 281.
20. Crowell, J. M. and Walker, J. C., in *Proc. 5th Int. Conf. on Mössbauer Spectroscopy*, ed. M. Hucl and T. Zemcik. Czechoslovak Atomic Energy Commission Nuclear Information Center, Praha, 1975, p. 289.
21. Kachi, S., Bando, Y. and Higuchi, S., *Japan J. appl. Phys*., 1962, **1**, 307.
22. Ron, M., in ed. R. L. Cohen, *Applications of Mössbauer Spectroscopy*, Vol. II. Academic Press, New York, 1980, p. 335.
23. Bauer, Ph., Uwakweh, O. N. C. and Genin, J. M. R., *Hyp. Int*., 1988, **41**, 555.